Dalton Transactions

PAPER

Influence of Gd^{3+} co-doping on structural property of $CaMoO_4$:Eu nanoparticles†

Cite this: *Dalton Trans.*, 2014, **43**, 4770

B. P. Singh,[a] A. K. Parchur,*[b] R. S. Ningthoujam,[c] A. A. Ansari,[d] P. Singh[a] and S. B. Rai[b]

A facile auto-combustion route is used for the synthesis of Gd^{3+} (2, 5, 7 and 10 at%) co-doped $CaMoO_4$:Eu nanoparticles. X-ray diffraction study suggests that as-prepared samples have extra impurity phases in addition to main tetragonal phase of $CaMoO_4$, and such extra phases decrease as the annealing temperature increases from 600 to 900 °C. The crystal structure has been analysed using Rietveld program. It has space group $I4_1/a$ (88) and Z = 4 (number of $CaMoO_4$ formula units per unit cell). Average crystallite sizes of as-prepared, 600 and 900 °C annealed samples for 2 at% Gd^{3+} are found to be ~33, 48 and 61 nm, respectively. The lattice strains of 5 at% Gd^{3+} co-doped $CaMoO_4$:Eu for as-prepared and 900 °C are 0.001 and 0.002, respectively. Fourier transform infrared spectroscopy gives the absorption bands at ~815 and 427 cm^{-1}, which are related to asymmetric stretching and bending vibrations of MoO_4^{2-} tetrahedron. Particle morphology is studied using scanning and transmission electron microscopy (SEM and TEM), and aggregation of particles is found. X-ray photoelectron spectroscopy (XPS) is utilized to examine the oxidation states of metal ions/oxygen and oxygen ion vacancies in Gd^{3+} co-doped $CaMoO_4$:Eu. With an increase in Gd^{3+} concentration, peaks corresponding to the Gd^{3+} ($2p_{3/2}$ and $2p_{5/2}$) binding energy could be detected.

Received 6th October 2013,
Accepted 1st December 2013

DOI: 10.1039/c3dt52786g

www.rsc.org/dalton

1. Introduction

Recently, alkaline-earth metal tungstate and molybdate (scheelite type, ABO_4, A = Ca^{2+}, Sr^{2+}, Mg^{2+} and Ba^{2+}; B = Mo and W) based derivatives are important host materials for rare-earth-doped phosphors because of their excellent optical and physical properties such as excellent strength, chemical and thermal stability, high decomposition temperature and multicolor range from blue to green–yellow–red.[1–5] Among the alkaline-earth metal molybdates, $CaMoO_4$ (having space group $I4_1/a$ and point group symmetry C_{4h}^6 with a tetragonal structure) has been used in solid-state lasers, scintillators in medical devices, solar cells and fiber-optic communication.[1–7] In $CaMoO_4$, Mo^{6+} is coordinated by four oxygen atoms in tetrahedral symmetry to form MoO_4 and Ca is coordinated by 8 oxygen atoms to form CaO_8.[5–8] The [MoO_4^{2-}] tetrahedron unit efficiently absorbs light with a higher absorption cross section near the UV region and its photoluminescence shows a broad visible range. The photoluminescence of $CaMoO_4$ doped with different lanthanide ions has been studied in order to obtain different colours.[1–7]

Nanomaterials have been synthesized in the form of nanorods, sheets, wires, nanopores and core–shell.[9–12] Lanthanide (Ln^{3+}) doped inorganic nanomaterials are used in luminescence applications because of their resistance to photobleaching, superior photochemical stability, sharp emission bands, persistent photoluminescence lifetime, high chemical stability and low toxicity.[13] Moreover, Ln^{3+} ions such as Gd^{3+} have a large number of unpaired electrons in the 4f orbitals, which can change the relaxation time of surrounding water protons when Ln^{3+} doped nanomaterials are dispersed in water. Thus, these are also used as magnetic resonance imaging (MRI) contrast agents in medical diagnostics.[14,15] There are reports on enhancement of luminescence by core–shell, co-doping and energy transfer processes.[16–19] Therefore, systematic research on the synthesis protocol, structure and its resultant effects on phosphor characteristics is necessary and worthy of pursuit. Moreover, the influence of Gd^{3+} incorporation on the structural and luminescence properties of $CaMoO_4$:Eu has not been explored in the literature in much detail. Many synthesis processes have been reported by different groups to synthesize $CaMoO_4$ with or without Ln^{3+} ions *via* Czochralski, conventional solid state reaction, sol–gel, hydrothermal, co-precipitation and polyol methods.[5,20] Auto-combustion methods have been proven to be very much

[a]*Department of Physics, Indian Institute of Technology (BHU), Varanasi, 221005, India*
[b]*Department of Physics, Banaras Hindu University, Varanasi, 221005, India. E-mail: kareemskpa@hotmail.com, ak.parchur@usu.edu*
[c]*Chemistry Division Bhabha Atomic Research Centre, Mumbai, 400085, India*
[d]*King Abdullah Institute for Nanotechnology, King Saud University, Riyadh, 11451, Saudi Arabia*

†Electronic supplementary information (ESI) available. See DOI: 10.1039/c3dt52786g

effective as they have a wide range of flexibility in the selection of fuels and a rapid cooling process which hinders the nucleation growth of the crystallites, enabling non-agglomerated nanocrystals of high purity with a nano-size regime. This methodology makes it possible to prepare nanomaterial with versatile compositions of different concentrations which is easily doped with various ions.[21]

In this work, we have prepared Gd^{3+} (0, 2, 5, 7 and 10 at%) co-doped $CaMoO_4$:Eu nanoparticles *via* an efficient combustion technique. Here, the urea–nitrate combustion synthesis is used. For the optimal Eu^{3+} concentration (2 at% in our case), the effect of Gd^{3+} co-doping on structure, chemical binding energies and morphology of $CaMoO_4$:Eu has been investigated in detail for as-prepared samples and samples annealed at 600 and 900 °C.

2. Experimental

2.1. Sample preparation

A combustion synthesis route was employed in order to synthesize the nanophosphors at lower temperature with high chemical homogeneity. $CaCO_3$ (99.99%, Sigma Aldrich), Eu_2O_3 (99.99%, Alfa Aesar), Gd_2O_3 (99.99%, Alfa Aesar) and $(NH_4)_6Mo_7O_{24}{\cdot}4H_2O$ (99%, Alfa Aesar) were used as starting materials. In a typical synthesis process (*e.g.* 2 at% Gd^{3+}, 2 at% Eu^{3+} doped $CaMoO_4$), 0.343 g of $CaCO_3$, 0.631 g of $(NH_4)_6Mo_7O_{24}{\cdot}4H_2O$, 0.126 g of Eu_2O_3 and 0.129 g of Gd_2O_3 were dissolved together in 2 ml of 1 M nitric acid (HNO_3). The mixture was heated at 80 °C to remove excess acid and this process was repeated at least five times with addition of 5 ml of doubled distilled water. A transparent solution was obtained after 1 hour. $(NH_4)_6Mo_7O_{24}{\cdot}4H_2O$ was dissolved in 20 ml of deionised water. To this solution, 2 g of urea was added to adjust the pH of the solution to between 8 and 9 and the solutions was placed under sonication for 30 min. This was added to the above solution drop-wise and stirred for 2–3 h. A whitish gel-like precipitate was obtained. This was placed in a furnace at ~250 °C for 30 min for auto combustion to take place. The powder sample obtained was denoted as the as-prepared sample (ASP). ASP samples were divided into three portions. One sample was annealed at 600 °C, the second at 900 °C for 4 h in ambient atmosphere at the rate of 2 °C min^{-1} in programmable electrical furnace and the remaining third part was kept as such.

2.2. Characterization techniques

Structural confirmation of the phosphors was identified by X-ray diffraction (XRD) using a Rigaku miniflex-II diffractometer equipped with a Ni filter using Cu K_α radiation (1.5405 Å) at ~30 kV and ~15 mA in the range $10 \leq 2\theta \leq 70°$ with a step size of $\Delta 2\theta = 0.02°$. The Fourier transform infrared (FTIR) spectra of the samples were recorded on a Perkin-Elmer 580 B IR spectrometer using the KBr pellet method in the range 4000–400 cm^{-1}. A sample was mixed with KBr (Sigma Aldrich, 99.99%) in 1 : 5 wt% ratio and a transparent pellet was prepared. The chemical binding energies of the respective ions in the samples were measured using X-ray photoelectron spectroscopy (XPS) SPECS, Germany (Mg K_α X-ray source, $h\nu$ = 1253.6 eV). Differential thermal (DT) and thermo-gravimetric (TG) analyses of the samples were carried out with a Material Analysis and Characterization TG-DTA 2000 with a heating rate of 5 °C min^{-1}. The morphology of the synthesized powder samples was further examined by field emission scanning electron microscopy (FESEM, JSM-6700, model JEOL, Japan). A coating of osmium was sprayed on the sample surfaces using a Hitachi (Japan) fine coat ion sputter E-1010 unit to avoid the expected charging of the specimens before FESEM observation was performed each time. Field emission transmission electron microscopy (FE-TEM) equipped with energy disperse X-ray spectroscopy, EDX (FETEM, JEM-2100F, JEOL, Japan) operating at an accelerating voltage of 200 kV was employed for the inspection of the morphology of the samples. EDX analysis was used to confirm the presence of the constituent elements in the sample. For the TEM measurement, a small amount of Gd^{3+} co-doped $CaMoO_4$:Eu was dispersed in the methanol and placed under sonication for 30 min. A few drops of suspended monodispersed colloidal solution were put over a carbon coated copper grid. Measurements were performed on these grids after drying the samples naturally.

3. Results and discussion

3.1. Structural analysis

3.1.1. XRD study. XRD patterns of ASP Gd^{3+} (0, 2, 5 7 and 10 at%) co-doped sample of $CaMoO_4$:Eu are shown in Fig. 1(a). It is evident from the figure that even as-prepared (ASP) samples show highly crystalline behaviour with tetragonal structure. All diffraction peaks match well with JCPDS card no. 29-0351 (a = 5.226 Å, c = 11.43 Å and V = 312.17 $Å^3$). In the case of Gd^{3+} (2, 5, 7 and 10 at%) co-doped ASP samples, some extra XRD peaks (marked with #) are observed at 2θ = ~17, 19.47, 25.98, 27.39, 35.48 and 42.7°. Such peaks do not match with JCPDS card no. 29-0351. The intensity of these extra peaks increases as the doping concentration of Gd^{3+} increases. Also, some extra peaks are found at ~23.3, 25.6 and 26.9° for 10 at% Gd^{3+} co-doped samples of $CaMoO_4$:Eu annealed at 600 °C. These extra peaks may be due to the $MoO_n{\cdot}mH_2O$ (where m and n are numbers), carbonate, water complexes, Gd–Eu–O related compounds, or Eu^{3+} oxides present in the sample. These phases are not identified in this study. Similar observations have been reported for Tb^{3+} doped $CaMoO_4$.[5] However, in the case of the 900 °C annealed samples, no other traces of impurity phases were observed. However, the intensities of diffraction peaks slightly decrease at higher Gd^{3+} co-doping concentrations. Lattice parameters of typical 5 at% Gd^{3+} co-doped $CaMoO_4$:Eu for ASP are a = 5.239 Å, c = 11.392 Å, V = 313.07 $Å^3$ and for 900 °C annealed samples are a = 5.226 Å, c = 11.437 Å and V = 312.37 $Å^3$. Unit cell volumes calculated for ASP samples are slightly high because of the broadness of the peaks as compared to the standard JCPDS card no. 29-0351. Samples annealed at ~600 and 900 °C, which are shown in

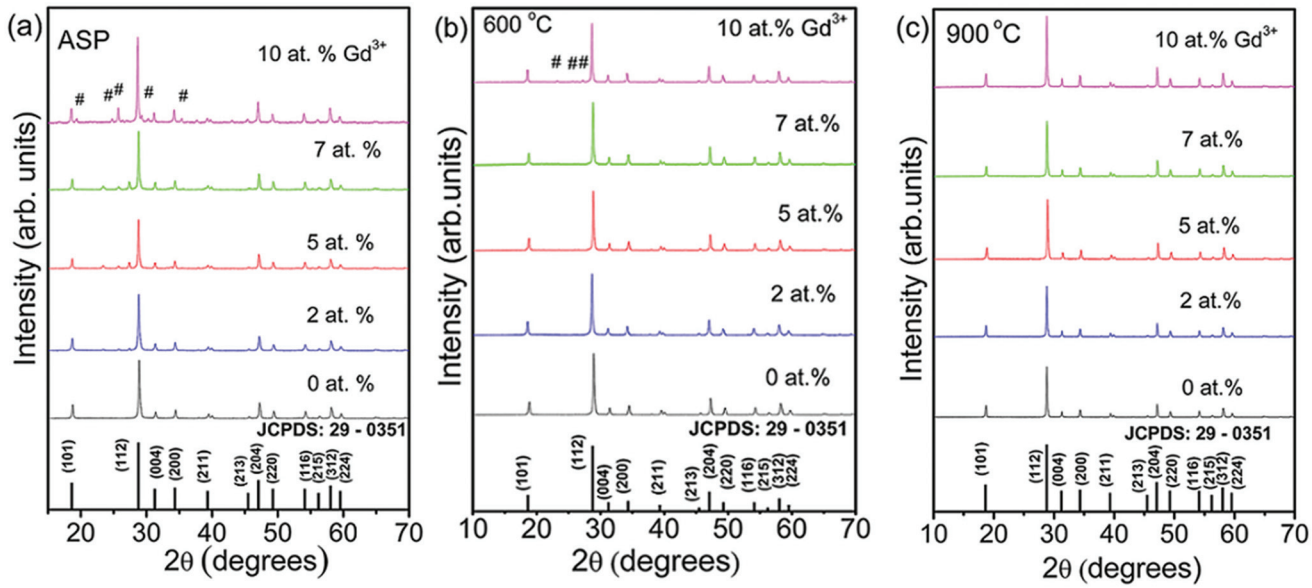

Fig. 1 (a), (b) and (c) XRD patterns of Gd^{3+}(0, 2, 5, 7 and 10 at%) co-doped $CaMoO_4$:Eu for ASP, 600 and 900 °C samples, respectively. Atomic percentage of Gd^{3+} is given in figure itself. The symbol # represents the extra phase evolution.

Fig. 1(b) and (c), respectively, show slightly higher crystalline behaviour than the ASP samples. The average crystallite size of the samples was calculated by using Scherrer formula,

$$D = \frac{k\lambda}{\beta_{hkl}\cos(\theta)} \quad (1)$$

where D is average crystallite size, $k = 0.89$, λ is wavelength, θ is the Bragg's diffraction angle of the planes and β_{hkl} is the corrected full width at half maximum (FWHM). For β_{hkl} correction, β_{inst} (FWHM due to instrument) is removed using an Si standard. The average crystallite size determined using the Scherrer formula for the 2 at% Gd^{3+} co-doped $CaMoO_4$:Eu of ASP, 600 and 900 °C annealed samples are found to be ~33, 48 and 61 nm, respectively. The average crystallite size of the samples annealed at ~600 and 900 °C is found to increase with the Gd^{3+} doping concentration. Structure refinement of Gd^{3+} (0, 2, 5 7 and 10 at%) co-doped $CaMoO_4$:Eu samples annealed at ~600 and 900 °C was carried out using FullProf software.[22] The peak profiles were modelled using the Pseudo-Voigt function while the background was described in terms of a six coefficient polynomial. R_{wp} (weighted-pattern factor) and S (goodness-of-fit) parameters were used as numerical criteria of the quality of fit to experimental diffraction data. Rietveld refinement patterns of Gd^{3+} (0, 2, and 10 at%) co-doped $CaMoO_4$:Eu, for 900 °C are shown in Fig. 2(a–c). The Wyckoff positions of atoms based on space group $I4_1/a$ (88) and $Z = 4$ (number of $CaMoO_4$ formula units per unit cell) in $CaMoO_4$ unit cell are:[8]

Ca: (4b: 0, 1/4, 5/8)

Mo: (4a: 0, 1/4, 1/8)

O: (16f: x, y, z)

The Bragg reflections and the difference in observed and calculated intensities are shown in the figure itself. Refinement patterns of 5 and 7 at% Gd^{3+} co-doped $CaMoO_4$:Eu for 900 °C are given in Fig. S1(a) and (b) (ESI†). Moreover, refinement patterns of Gd^{3+} (0, 2, 5, 7 and 10 at%) co-doped samples of $CaMoO_4$:Eu annealed at 600 °C are shown in Fig. S2(a)–(e) (ESI†). The crystal structure and symmetry resembled to that of its simplified 3D polyhedral representation, shown in Fig. 2(d), which demonstrates the presence of high inversion symmetry in the lattice. $CaMoO_4$ is a derivative of ABO_4 (A = Ca, Ba, Sr, Pb and B = Mo, W) with tetragonal scheelite structure having body centred inversion symmetry. A and B sites show S_4 point symmetry while its crystal structure comprises two building block units namely, Eu/Gd/CaO_8 polyhedra and MoO_4 tetrahedra. In the c direction, the Eu/Gd/CaO_8 polyhedron shares four of its edges with four other Eu/Gd/CaO_8 polyhedrons through oxygen atoms. The oxygen atoms share co-ordination among Eu/Gd/CaO_8 polyhedra and MoO_4 tetrahedra, respectively. Observed lattice parameters after Rietveld refinement, cell volume and average crystallite size for 600 and 900 °C samples for Gd^{3+} (0, 2, 5, 7 and 10 at%) co-doped $CaMoO_4$:Eu samples are listed in Table 1. It is found that the cell volume slightly increases after Gd^{3+} incorporation in $CaMoO_4$:Eu for 900 °C annealed samples in comparison to the samples annealed at 600 °C. This is may be due to ionic radii mismatch of Ca^{2+} ions with Gd^{3+}/Eu^{3+}. Ionic radii of Eu^{3+} (1.06 Å) and Gd^{3+} (1.05 Å) are similar to Ca^{2+} (1.12 Å) based on 8 coordination number (CN) [CaO_8] and Mo^{6+} has ionic radius of 0.42 Å in [MoO_4]. Therefore, Eu^{3+} and Gd^{3+} are supposed to occupy Ca^{2+} sites in spite of the charge imbalance.[8,23] The micro-strain has been calculated for Gd^{3+} co-doped $CaMoO_4$ for ASP and 900 °C annealed samples using the Williamson–Hall[24] formula, given as:

$$\frac{\beta_{hkl}\cos\theta}{\lambda} = \frac{1}{D_{hkl}} + (\varepsilon_{hkl})\frac{\sin\theta}{\lambda} \quad (2)$$

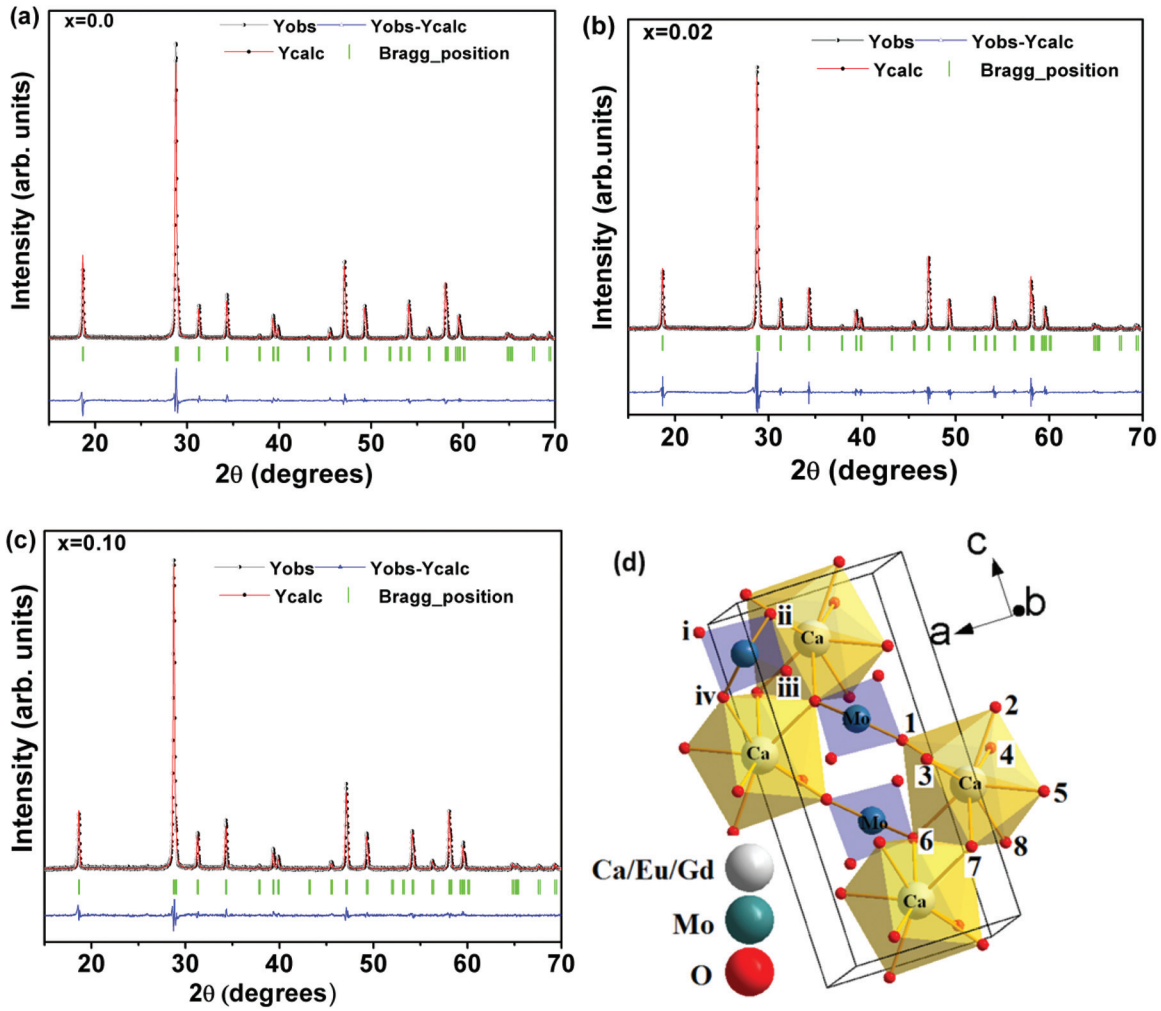

Fig. 2 (a), (b), (c) Rietveld plot of 0, 2 and 10 at% Gd^{3+} co-doped $CaMoO_4$:Eu samples annealed at 900 °C and (d) simplified polyhedral representation of Gd^{3+} co-doped $CaMoO_4$:Eu having both [CaO_8] and [MoO_4] clusters.

Table 1 Calculated values of *a*, *c*, *V* and *D* for Gd^{3+} (0, 2, 5, 7 and 10 at%) co-doped $CaMoO_4$:Eu at 600 °C and 900 °C

	600 °C				900 °C			
Gd^{3+}	*a*	*c*	*V*	*D*	*a*	*c*	*V*	*D*
0	5.224(2)	11.446(5)	312.11(19)	38	5.224(2)	11.439(4)	312.14(18)	59
2	5.223(2)	11.437(5)	311.97(02)	48	5.225(2)	11.434(3)	312.15(16)	61
5	5.226(2)	11.440(5)	312.28(02)	52	5.227(2)	11.437(5)	312.37(22)	62
7	5.226(2)	11.433(5)	312.25(19)	54	5.227(2)	11.431(4)	312.31(17)	71
10	5.226(2)	11.442(5)	312.16(21)	57	5.227(2)	11.429(5)	312.27(19)	69

where β_{hkl} is the full width at half maximum (FWHM) of X-ray patterns, θ is the Bragg's diffraction angles, λ is the wavelength of X-rays, D_{hkl} is the effective crystallite size and ε_{hkl} is the micro-strain. The instrumental broadening (ε_{ins}) is removed by using Si standard. Micro-strain is calculated for 0, 5 and 10 at% Gd^{3+} co-doped $CaMoO_4$:Eu and the values are found to be ~0.0014, 0.0017 and 0.0027 for ASP and ~0.0016, 0.0023 and ~0.0029 for 900 °C annealed samples. It has been inferred from the strain data that it increases with an increase in Gd^{3+} concentration. A positive slope value (ε_{hkl}) indicates the presence of tensile strain acting on the system.[12] Dutta *et al.* have reported recently the variation in strain (0.001–0.003) in Dy^{3+} doped $CaMoO_4$. It is found that strain increases with Dy^{3+} concentration, and being relaxed by co-doping of K^+ ions in $CaMoO_4$.[25]

It is observed that the pattern intensity of Gd^{3+} co-doped $CaMoO_4$:Eu is slightly less than $CaMoO_4$:Eu samples, which is due to defects created in Gd^{3+} co-doped $CaMoO_4$:Eu. Extra

phases demonstrate the solubility limit of Gd^{3+} and Eu^{3+} ions in host lattice. It expected that for up to 2 at% of Eu^{3+} and up to 10 at% Gd^{3+} charge compensation occurs for Ca^{2+} and oxygen ion vacancies. In the present study, nanophosphors are synthesized without any charge compensation of ions. The crystal structure are still consistent with scheelite phase for Gd^{3+} content up to 10 at% for 600 and 900 °C annealed samples. Charge loss may be compensated for by Ca^{2+} vacancies (V''_{Ca}). The defect equation mechanism for the Ca^{2+} vacancies can be proposed as:

$$Eu_2O_3(CaO) \rightarrow 2Eu_{Ca}^{\bullet} + 3O_o^{x} + V''_{Ca}$$

and

$$Gd_2O_3(CaO) \rightarrow 2Gd_{Ca}^{\bullet} + 3O_o^{x} + V''_{Ca},$$

where O_o^{x} is oxygen ion vacancies.

In other words two Eu^{3+} or two Gd^{3+} ions must replace three Ca^{2+} sites to maintain charge balance and hence one V''_{Ca} is created. Ionic radii mismatch among the Ca^{2+}, Eu^{3+} and Gd^{3+} are supposed to be responsible for the vacancy generation of V''_{Ca} and creation of other point defects in the lattice. Similar behaviour has been reported for Bi^{3+} co-doped $CaMoO_4$:$5Eu^{3+}$.[26]

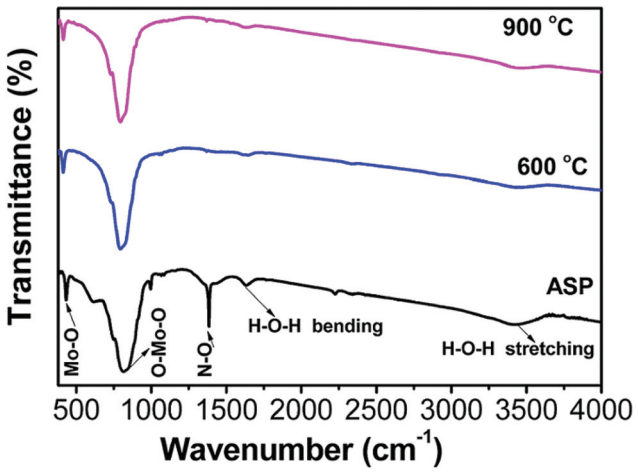

Fig. 3 FTIR spectra of ASP, 600 and 900 °C annealed samples of 5 at% Gd^{3+} co-doped $CaMoO_4$:Eu.

3.1.2. FTIR study. FTIR spectra of the ASP, 600 and 900 °C annealed samples of 5 at% Gd^{3+} co-doped $CaMoO_4$:Eu in the range 400–4000 cm^{-1} are shown in Fig. 3. Infrared absorption spectra show all the expected vibrational modes of calcium molybdate, which confirms the phase purity of the materials. Group theory calculations show that there are 26 modes of vibrations (Raman and infrared) for the scheelite type structure, which can be represented as:[27]

$$\Gamma_{(\text{Raman+Infrared})} = 3A_g + 5A_u + 5B_g + 3B_u + 5E_g + 5E_u \quad (3)$$

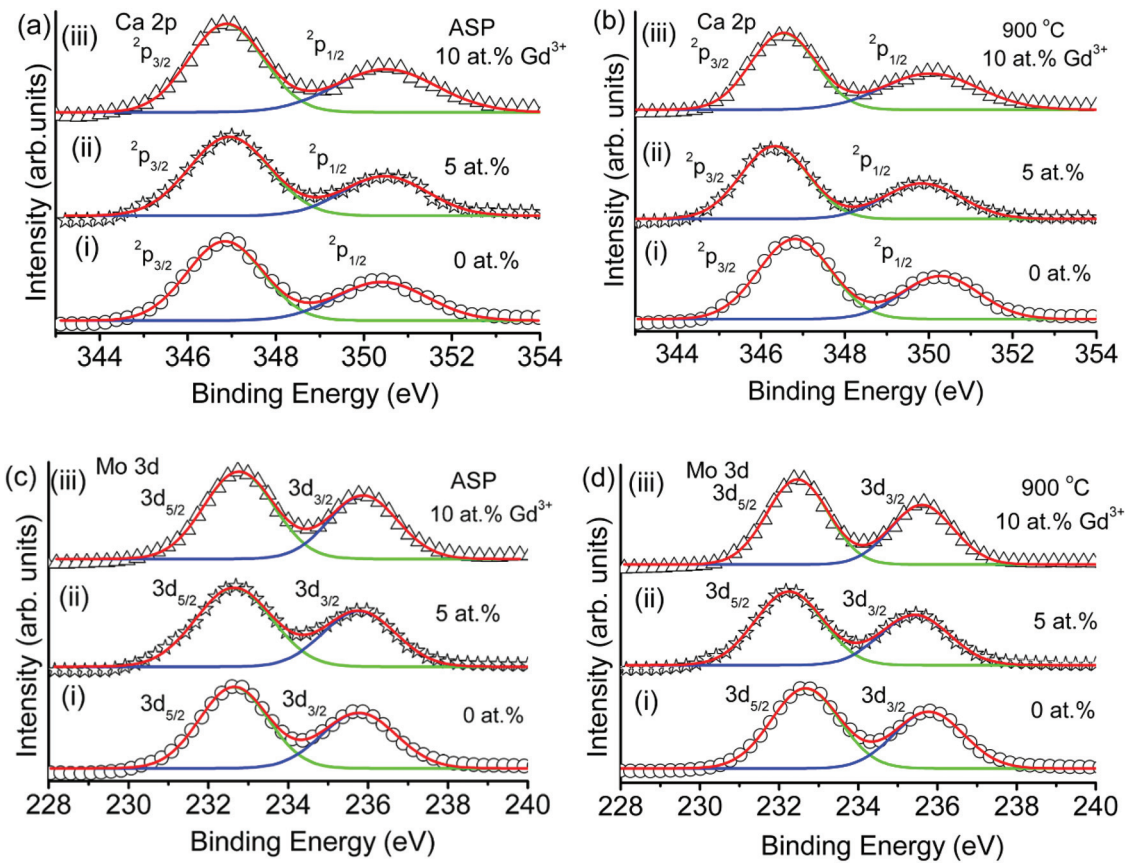

Fig. 4 XPS spectra of as-prepared and 900 °C annealed samples of 0, 5 and 10 at% Gd^{3+} co-doped $CaMoO_4$:Eu. Peaks corresponding to the core binding energies of individual elements *viz.*, Ca and Mo are shown in (a)–(d).

where A_g, B_g and E_g are Raman-active modes. There are 13 Raman active modes observed for the $CaMoO_4$, which is represented by equation as:[28]

$$\Gamma_{(\text{Raman})} = 3A_g + 5B_g + 5E_g \quad (4)$$

and eight infra-red active modes, given as:[29]

$$\Gamma_{(\text{infrared})} = 4A_u + 4E_u \quad (5)$$

Infrared bands at ~1652 and 3419 cm^{-1} correspond to bending and stretching vibrational modes of absorbed water molecules on the surface of nanoparticles.[30] Observed absorption pattern intensity decreases as the annealing temperature increases. Absorption peaks appearing at ~815 cm^{-1} occur due to the asymmetric stretching vibration of O–Mo–O vibration in the MoO_4^{2-} tetrahedron, while the peak at ~427 cm^{-1} occurs due to the bending vibration of Mo–O of the A_u mode.[31,32] It is observed that both O–Mo–O and Mo–O vibrations are slightly shifted towards lower wave number (~3–5 cm^{-1}) after annealing the samples at 600 and 900 °C, which infers the lattice expansion of the $CaMoO_4$ host. The red shifts in the A_u mode of vibration are responsible for lattice expansion in the host. A band arising at ~1383 cm^{-1} demonstrates the presence of N–O modes of vibration of HNO_3 used in the sample preparation. A similar observation was reported in Tb^{3+} doped $CaMoO_4$.[5]

3.1.3. XPS study. The oxidation states of the constituent elements present in sample can be identified using XPS. The XPS spectra of Ca, Mo and O core binding energy (BE) in ASP and 900 °C annealed samples of 0, 5 and 10 at% Gd^{3+} co-doped $CaMoO_4$:Eu are shown in Fig. 4 and 5. Whole spectra comprising core BE levels of Ca, Mo, O, Eu/Gd are shown in Fig. S3(a) (ESI†), obtained in the range of 0–1000 eV. Fig. 4(a) (i)–(iii) shows the XPS spectra of Ca (2p) for 0, 5 and 10 at% Gd^{3+} co-doped $CaMoO_4$:Eu ASP samples. For the Gd^{3+} free $CaMoO_4$:Eu sample, the peaks correspond to Ca (2p) with core BE ~346.84 ($2p_{3/2}$) and 350.39 eV ($2p_{1/2}$) and full width at half maximum (FWHM) ~1.7 and 2.0 eV. On increasing Gd^{3+} (5 and 10 at%) co-doping concentration, there are slight changes in BE values to higher eV. Moreover, the integrated intensity ratio of ($2p_{3/2}$) to ($2p_{1/2}$) (I_{Ca}) is found to be 1.76, 1.9 and 1.47 eV for 0, 5 and 10 at% Gd^{3+} co-doping, respectively. On annealing the sample at 900 °C, there is a slight decrease in BE of Ca($2p_{3/2}$) and Ca($2p_{1/2}$) by 0.25–0.47 eV for 0, 5 and 10 at% Gd^{3+} co-doped $CaMoO_4$:Eu samples, which is shown in Fig. 4(b) (i)–(iii); FWHM and I_{Ca} do not change significantly within the limits of the error bars. These results confirm the 2+ oxidation state of Ca. Fig. 4(c) (i) shows peaks at ~232.64 and 235.77 eV, which correspond to the core BE of Mo($3d_{5/2}$) and Mo($3d_{3/2}$), respectively, for the ASP Gd^{3+} free $CaMoO_4$:Eu sample. The integrated intensity ratios of ($3d_{5/2}$) to ($3d_{3/2}$) (I_{Mo}) are found to be 1.36, 1.49 and 1.39 eV for 0, 5 and 10 at% Gd^{3+} co-doping samples, respectively (Fig. 4(c) (i)–(iii)). There is no significant change in BE upon Gd^{3+} co-doping. Upon annealing the samples at 900 °C, BE are slightly shifted to lower eV by 0.17 to 0.47 eV (Fig. 4(d) (i)–(iii)). Also, I_{Mo} was found to be 1.39, 1.43 and 1.39 eV for 0, 5 and 10 at% Gd^{3+} co-doping

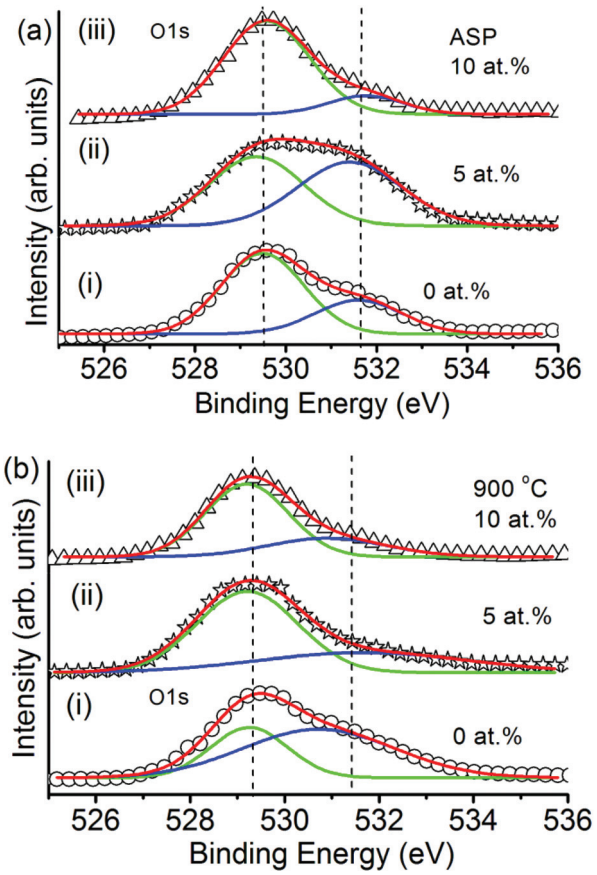

Fig. 5 XPS spectra of O1s for (a) ASP and (b) 900 °C annealed, Gd^{3+} (0, 5 and 10 at%) co-doped $CaMoO_4$:Eu.

samples, respectively. The lack of any significant change in the $3d_{3/2}$–$3d_{5/2}$ BE in the Mo spectral region suggests that Mo ions remain in the Mo^{6+} state. Similar behaviour was supported in the literature[33,34] for Ca–Bi–Mo oxide and for molybdenum phosphate glass. Notably, the peaks for Gd^{3+} and Eu^{3+} fall at ~141–148 eV so it is difficult to distinguish between $Eu^{3+}(4d_{3/2})$ and $Gd^{3+}(4d)$. A peak at ~141.1 eV corresponds to $Eu^{3+}(4d_{3/2})$ and no peak at ~127.1 eV corresponding to $Eu^{2+}(4d_{5/2})$ is observed. This confirmed that the high probability of presence of Eu^{3+} ion present in the sample and is also confirmed from excitation/emission study (not shown).[35a] Moreover, small peaks at 141.4 and 146.2 eV correspond to Gd($2p_{3/2}$) and Gd ($2p_{5/2}$), respectively.[35b] Typical XPS spectra showing core binding energy and intensity of Eu and Gd in 10 at% ASP Gd^{3+} co-doped $CaMoO_4$:Eu are shown in Fig. S4 (ESI†). The intensity of these peaks is very small for ASP and 900 °C annealed samples and increases with increase of Gd^{3+} concentration. This is may be due to presence of fewer Gd^{3+}/Eu^{3+} ions in the sample. In addition, O(1s) spectral regions have been used to obtain information regarding the presence of oxygen vacancies present in the sample (Fig. 5). Peaks were deconvoluted using a Gaussian function. In the case of the ASP Gd^{3+} free $CaMoO_4$:Eu sample, two peaks are well fitted at BE ~529.5 (P_1) and 531.6 eV (P_2) having FWHM ~1.8 and 1.82 eV, respectively. On increasing Gd^{3+} co-doping, the peak position slightly changes by

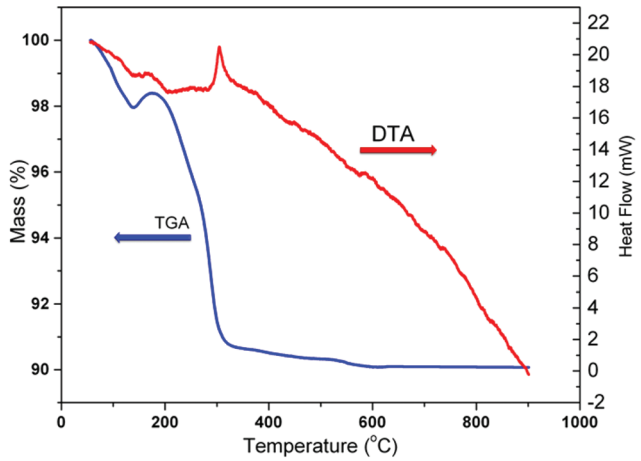

Fig. 6 TG-DTA curves of as-prepared precursor (ASP) for $CaMoO_4$:Eu in synthetic air.

±0.1–0.4 eV (Fig. 5(a)). Similar spectra are observed upon annealing the sample at 900 °C (Fig. 5(b)). The BE of the peaks is shifted by ~±0.26–0.76 eV with respect to corresponding ASP samples. Overall, peaks show an asymmetric nature on the higher BE side. Further, the relative area of P_2/P_1 of ASP and 900 °C annealed samples for 0, 5 and 10 at% Gd^{3+} co-doped $CaMoO_4$:Eu provides interesting features shown in Fig. S3(b) (ESI†). This is may be due to the defects and oxygen vacancies created on behalf of non-isovalent dopant. There are a few reports that indicate that the high energy side of the O(1s) peak arises due to hydroxyl groups –OH or other radicals on the sample surface, such as CO or CO_2.[36] However, the asymmetric behaviour at high energy peak (~530.5 eV) in an O1s spectrum is a signature of the presence of oxygen ion vacancy in the lattice.[37] It can be suggested that oxygen vacancies decrease with annealing the sample at high temperature.

3.1.4. DT-TGA study. Thermal decomposition of ASP $CaMoO_4$:Eu in air has been studied by thermogravimetric (TGA) and differential thermal analyses (DTA), shown in Fig. 6. The TG curve shows two distinct stages of weight loss. The first weight loss (~2%) step is observed between 55–140 °C, which is attributed to the removal of residual water molecules absorbed on the sample surface. The second weight loss (8%) is in the temperature range 140–600 °C, accompanied by an exothermic peak at 305 °C in the DTA curve which may be due to the further combustion of organic matrices such as hydrocarbons, carbonates and nitrates. Moreover, weight loss above ~600 °C becomes constant and thereafter no significant loss has been observed up to 900 °C. This demonstrates that combustion and decomposition of all organic constituent precursors in the samples have been completed below 600 °C.

3.1.5. SEM and TEM studies. Morphological aspects of the $CaMoO_4$:Eu nanophosphors of ASP, 600 and 900 °C are investigated by SEM and TEM. The typical SEM morphology of $CaMoO_4$:Eu nanophosphors of ASP, 600 and 900 °C heated samples are shown in Fig. 7(a)–(c), respectively. The scale bar indicated on each figure corresponds to 100 nm. In ASP, there are agglomerated particles, in which one particle contains

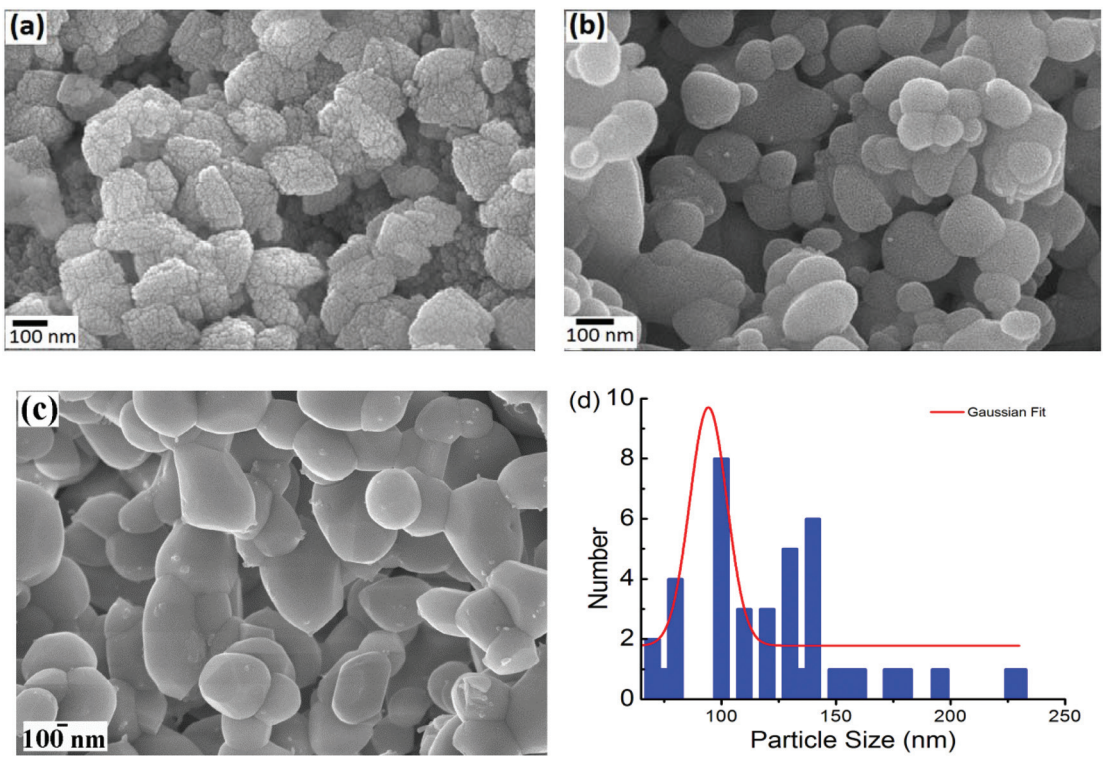

Fig. 7 FESEM images of micro-spherical particles $CaMoO_4$:Eu: (a) as-prepared, (b) annealed at 600 °C and (c) annealed at 900 °C. (d) Particle size distribution for 600 °C annealed sample.

many small crystallites. Each crystallite has 30–40 nm size. At 600 °C, particles are spherical in shape and the smallest particle has a size of 50–60 nm. At 900 °C, bigger aggregates of spherical particles are obtained and the smallest particle has size of 350–360 nm. It is observed that as the annealing temperature increases, the particle size increases. Particle size distribution histograms for 600 (Fig. 7(b)) and 900 °C (Fig. 7(c)) annealed samples are presented in Fig. 7(d) and Fig. S5 (ESI†), respectively. The mean diameters of the particles for 600 and 900 °C annealed $CaMoO_4$:Eu are found to be ~100 and ~500 nm, respectively, upon fitting the histogram with a Gaussian function.

A typical TEM micrograph of ASP 5 at% Gd^{3+} co-doped $CaMoO_4$:Eu is shown in Fig. 8(a). Many crystallites form an agglomerated particle. This is similar to the SEM observation. HRTEM of 5 at% Gd^{3+} co-doped $CaMoO_4$:Eu at 900 °C is used to calculate the *d* spacing and corresponding (*hkl*) plane, and is shown in Fig. 8(c). It confirms that maximum growth of the crystal has taken along the (101) plane and d_{101} = 4.5 Å. To check the growth direction of planes and their corresponding *d* spacing, we have analysed by taking various plane spots in HRTEM, as shown in Fig. S6 (ESI†) marked as (i), (ii), (iii) and (iv). From this, it is inferred that in most of the cases *i.e.* at (i), (ii) and (iii) spots, the *d* spacing is same as marked in Fig. 8(c). For region marked as (iv), some crystal growth takes place in (004) planes with spacing having 2.77 Å, which is shown in Fig. S6(c) (ESI†). Energy dispersive spectra (EDS) of ASP 5 at% Gd^{3+} co-doped $CaMoO_4$:Eu is shown in Fig. 8(b). EDS analysis reveals the presence of the most intense peaks of Mo along with calcium (Ca), oxygen (O), europium (Eu), gadolinium (Gd) and Cu peaks. The presence of Cu peaks in the EDS spectra are manifestation from the copper micrometer grids. Moreover, no other impurities were pronounced, indicating that Gd^{3+} co-doped $CaMoO_4$:Eu phosphors are chemically pure in composition *via* the auto combustion route.

4. Conclusions

Highly crystalline Gd^{3+} (0, 2, 5, 7 and 10 at%) co-doped $CaMoO_4$:Eu nanoparticles are synthesized *via* a facile auto-combustion route. In order to get the higher crystallinity, the ASP sample is heated at 600 and 900 °C. The tetragonal scheelite phase with space group $I4_1/a$ and Z = 4 is found. Extra

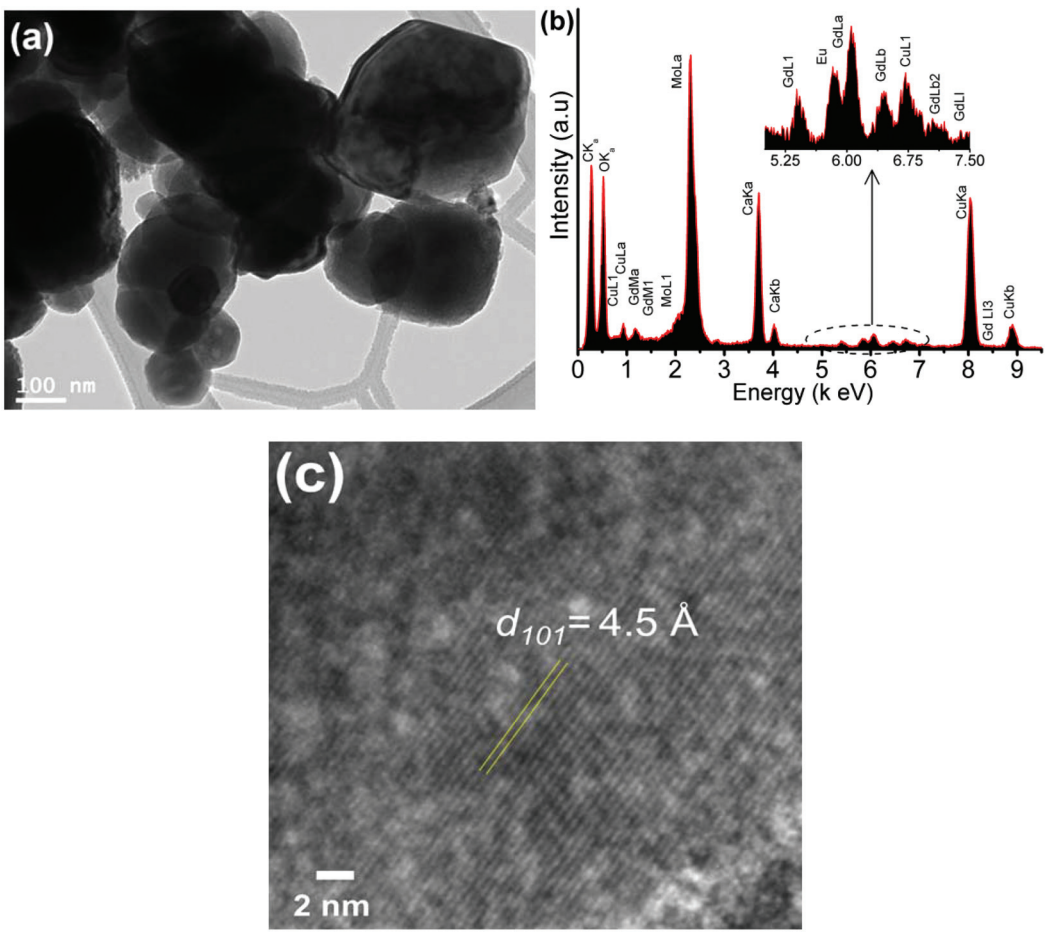

Fig. 8 (a) TEM image and (b) the elemental composition of a large area of ASP 5 at% Gd^{3+} co-doped $CaMoO_4$:Eu nanophosphors, which is verified by the presence of Ca, Mo, Eu and Gd peaks. Cu peak comes from the copper grid used for the electron microscopy analysis. (c) HRTEM image of 5 at% Gd^{3+} co-doped $CaMoO_4$:Eu at 900 °C.

peaks in XRD patterns are found in the case of ASP and 600 °C and are not present in 900 °C. The FTIR spectrum shows bands at ~815 cm^{-1} and 427 cm^{-1}, which are due to asymmetric stretching and bending vibrations of O–Mo–O of MoO_4^{2-} tetrahedra, respectively. From XPS study, Ca is found to be in the +2 oxidation state, while Mo, Eu and Gd are found to be in the +6, +3 and +3 oxidation states, respectively. The core binding energy peak at ~141.1 eV corresponds to $Eu^{3+}(4d_{3/2})$. No peak at ~127.1 eV, corresponding to $Eu^{2+}(4d_{5/2})$, is observed. This supports the high probability of Eu^{3+} being present in the samples. The particle size increases with annealing.

Acknowledgements

One of the authors (B. P. Singh) is thankful to Ministry of Human Resource and Development (MHRD) for providing financial support in the form of teaching assistantship.

References

1 G. S. R. Raju, E. Pavitra, Y. H. Ko and J. S. Yu, *J. Mater. Chem.*, 2012, **22**, 15562.
2 A. K. Parchur, R. S. Ningthoujam, S. B. Rai, G. S. Okram, R. A. Singh, M. Tyagi, S. C. Gadkari, R. Tewari and R. K. Vatsa, *Dalton Trans.*, 2011, **40**, 7595.
3 E. Cavalli, P. Boutinaud, R. Mahiou, M. Bettinelli and P. Dorenbos, *Inorg. Chem.*, 2010, **49**, 4916.
4 S. Mahlik, M. Behrendt, M. Grinberg, E. Cavalli and M. Bettinelli, *J. Phys.: Condens. Matter*, 2013, **25**, 105502.
5 A. K. Parchur, A. I. Prasad, A. A. Ansari, S. B. Rai and R. S. Ningthoujam, *Dalton Trans.*, 2012, **41**, 11032.
6 V. S. Marques, L. S. Cavalcante, J. C. Sczancoski, A. F. P. Alcantara, M. O. Orlandi, E. Moraes, E. Longo, J. A. Varela, M. S. Li and M. R. M. C. Santos, *Cryst. Growth Des.*, 2010, **10**, 4752.
7 V. M. Longo, L. S. Cavalcante, E. C. Paris, J. C. Sczancoski, P. S. Pizani, M. S. Li, J. Andres, E. Longo and J. A. Varela, *J. Phys. Chem. C*, 2011, **115**, 5207.
8 A. K. Parchur and R. S. Ningthoujam, *Dalton Trans.*, 2011, **40**, 7590.
9 S. Acharya, U. K. Gautam, T. Sasaki, Y. Bando, Y. Golan and K. Ariga, *J. Am. Chem. Soc.*, 2008, **130**, 4594.
10 K. Ariga, A. Vinu, Y. Yamauchi, Q. Ji and J. P. Hill, *Bull. Chem. Soc. Jpn.*, 2012, **85**, 1.
11 A. Vinu and K. Ariga, *Adv. Porous Mater.*, 2013, **1**, 63.
12 A. Kar and A. Patra, *Nanoscale*, 2012, **4**, 3608.
13 B. K. Gupta, V. Rathee, T. N. Narayanan, P. Thanikaivelan, A. Saha, Govind, S. P. Singh, A. A. Marti and P. M. Ajayan, *Small*, 2011, **7**, 1767.
14 H. Guo, Z. Li, H. Qian, Y. Hu and I. N. Muhammad, *Nanotechnology*, 2010, **21**, 125602.
15 N. O. Nunez, S. Rivera, D. Alcantara, J. M. Fuente, J. G. Sevillano and M. Ocana, *Dalton Trans.*, 2013, **42**, 10725.
16 A. Podhorodecki, M. Bański, J. Misiewicz, J. Serafińczuk and N. V. Gaponenko, *J. Electrochem. Soc.*, 2010, **157**, H628.
17 A. Podhorodecki, G. Zatryb, J. Misiewicz, D. Kaczmarek, J. Domaradzki and A. Borkowska, *J. Electrochem. Soc.*, 2009, **156**, H214.
18 A. Podhorodecki, J. Misiewicz, F. Gourbilleau and C. Dufour, *Electrochem. Solid-State Lett.*, 2010, **13**, K26.
19 A. Podhorodecki, R. Kudrawiec, M. Nyk, J. Misiewicz and W. Strek, *Opt. Mater.*, 2009, **31**, 1252.
20 S. Yu, Z. Lin, L. Zhang and G. Wang, *Cryst. Growth Des.*, 2007, **7**, 7595.
21 Z. Qiu, Y. Zhou, M. Lu, J. Zhou, A. Zhang, Z. Yang and Q. Ma, *Nanotechnology*, 2007, **17**, 495705.
22 J. Rodriguez- Carvajal, *FULLPROF, a Rietveld and pattern matching analysis program*, Laboratoire Leon Brillouin (CEA-CRNS), Paris, France.
23 R. D. Shanon, *Acta Crystallogr., Sect. A: Cryst. Phys., Diffr., Theor. Gen. Cryst.*, 1976, **32**, 751.
24 A. Kar, A. Dutta and A. Patra, *J. Mater. Chem.*, 2010, **20**, 916.
25 S. Dutta, S. Som and S. Sharma, *Dalton Trans.*, 2013, **42**, 9654.
26 S. Yan, J. Zhang, X. Zhang, S. Lu, X. Ren, Z. Nie and X. Wang, *J. Phys. Chem. C*, 2007, **111**, 13256.
27 D. L. Rousseau, R. P. Bauman and S. P. S. Porto, *J. Raman Spectrosc.*, 1981, **10**, 253.
28 S. P. S. Porto and J. F. Scott, *Phys. Rev.*, 1967, **157**, 716.
29 A. Golubovic, R. Gajic, Z. D. Mitrovic and S. Nikolick, *J. Alloys Compd.*, 2006, **415**, 16.
30 M. N. Luwang, R. S. Ningthoujam, Jagannath, S. K. Srivastava and R. K. Vatsa, *J. Am. Chem. Soc.*, 2010, **132**, 2759.
31 F. Lei and B. Yan, *J. Solid State Chem.*, 2008, **181**, 855.
32 P. Yang, C. Li, W. Wang, Z. Quan, S. Gai and J. Lin, *J. Solid State Chem.*, 2009, **182**, 2510.
33 S. I. Woo, J. S. Kim and H. K. Jun, *J. Phys. Chem. B*, 2004, **108**, 8941.
34 G. D. Khattak, M. A. Salim, A. S. Al. Harthi, D. J. Thompson and L. E. Wenger, *J. Non-Cryst. Solids*, 1997, **212**, 180.
35 (*a*) B. P. Singh, A. K. Parchur, R. S. Ningthoujam, A. A. Ansari, P. Singh and S. B. Rai, *Dalton Trans.*, 2014, DOI: 10.1039/c3dt53408a; (*b*) L. Zhou, Z. Gu, X. Liu, W. Yin, G. Tian, L. Yan, S. Jin, W. Ren, G. Xing, W. Li, X. Chang, Z. Hu and Y. Zhao, *J. Mater. Chem.*, 2012, **22**, 966.
36 L. R. Shah, B. Ali, H. Zhu, W. G. Wang, Y. Q. Song, H. W. Zhang, S. I. Shah and J. Q. Xiao, *J. Phys.: Condens. Matter*, 2009, **21**, 486004.
37 A. K. Parchur, A. I. Prasad, S. B. Rai, R. Tewari, R. K. Sahu, G. S. Okram, R. A. Singh and R. S. Ningthoujam, *AIP Adv.*, 2012, **2**, 032119.

